Forever young: how AHL15 delays developmental phase transitions to prevent ageing in plants

Luden, T.

Chapter 5

AHL15 modulates gene expression independently of chromatin accessibility and histone modifications

Thalia Luden[1], Jihed Chouaref[2], Remko Offringa[1]

[1] Plant Developmental Genetics, Institute of Biology Leiden, Leiden University, Sylviusweg 72, 2333 BE Leiden, the Netherlands

[2] Annogen, Science Park 406, 1098 XH Amsterdam, the Netherlands

Abstract

In recent years, members of the *AT-HOOK MOTIF NUCLEAR LOCALIZED (AHL)* gene family have been shown to play important roles in plant development. One member of this family, *AHL15*, enhances plant longevity when overexpressed by strongly repressing several ageing-related developmental switches, but its direct target genes and the manner with which it regulates their expression remained unknow so far. In this study we identified the genome-wide DNA binding sites of AHL15, and show that AHL15 binds throughout the genome at AT-rich regions near the transcription start- and end sites in regions depleted of epigenetic marks without recognizing a specific sequence. We show that induction of AHL15 activity causes strong and rapid changes in transcription, with the majority of the differentially expressed genes being downregulated but without directly affecting chromatin accessibility, resulting in developmental defects. In addition, AHL15 binding to regions near the transcription start and end sites was enhanced at genes that were differentially expressed upon AHL15 induction, and was especially strong near the transcription start site of upregulated genes and near the transcription end site of downregulated genes. Finally, we show that AHL15 shares binding sites with the chromatin architectural protein GH1-HMGA2/HON5, which was previously shown to alter transcription by disrupting gene loop formation. Together, our findings suggest that AHL15 affects the expression of its target genes by regulating the 3D organization of chromatin.

Keywords: AHL15, aging, AT-hook proteins, chromatin architecture, gene looping

Introduction

In recent years, research on the plant-specific AT-HOOK MOTIF NUCLEAR LOCALIZED (AHL) protein family has shown that members of this plant-specific gene family have diverse roles in developmental processes, such as hypocotyl elongation, root architecture, somatic embryogenesis, vegetative phase change, flowering time, and longevity (Street et al., 2008; Zhou et al., 2013; Karami et al., 2020; Karami et al., 2021; Rahimi et al., 2022a). The *AHL* family is conserved in all land plants, with the size of the family varying between ten genes in *Physcomitrella patens* (moss), 29 in *Arabidopsis thaliana* (Arabidopsis), 20-26 in *Oryza sativa* (rice) and 47 in carrot (Kim et al., 2011; Zhao et al., 2014; Machaj and Grzebelus, 2021; Kumar et al., 2023). Despite the considerable size of this gene family, research on AHLs has emerged only in recent years, and much remains to be discovered about their function in development and gene regulation.

AHL proteins bind to the minor groove of AT-rich DNA via their AT-hook domain, which can also be found in other DNA-binding proteins such as the High-Mobility Group A (HMGA) family (Klosterman and Hadwiger, 2002; Fujimoto et al., 2004). The AHL family is subdivided into two clades (A and B) based on the structure and number of AT-hook domains: clade A members have a single, type A AT-hook domain, whereas clade B members have a type B AT-hook domain that is sometimes accompanied by a second AT-hook domain of the A type (Zhao et al., 2013; Zhao et al., 2014). In the nucleus, AHL proteins are thought to form heterotrimeric complexes and to jointly recruit other nuclear proteins via their PPC (Plant and Prokaryote Conserved) domains (Zhao et al., 2013). While single *ahl* mutants often show very mild phenotypes, such as a slightly accelerated flowering time (Karami et al., 2020; Rahimi et al., 2022a), more striking phenotypic defects can be observed when one of the characteristic AHL domains are mutated. Removal of the AT-hook domain *(ΔAT-hook)* causes loss of DNA binding, whereas deletion of a six amino acid sequence in the PPC domain *(ΔG)* or interference with the PPC domain function by fusion of the ǧ-glucuronidase (GUS) reporter protein reduces the capacity to recruit other nuclear proteins (Lin et al., 2007; Zhao et al., 2013; Karami et al., 2021). Such mutant AHL proteins have a strong dominant-negative effect on AHL function, as was shown by the inhibitory effect of *AHL15-ΔG* or *AHL15-GUS* on zygotic or somatic embryogenesis when expressed in a heterozygous *ahl15* +/- background (Karami et al., 2021), or by the *sob3-6* mutant which expresses a *ΔAT-hook* allele of *AHL29* and shows a significantly longer hypocotyl than either wild-type or *ahl29* knockout plants (Zhao et al., 2013). The phenotype of

these dominant-negative mutants and the high level of redundancy between *AHLs* indicates that the absence of an AHL protein can be compensated for by other AHLs, but that the incorporation of a defective AHL protein disrupts the function of the trimeric complex.

Due to the high redundancy between *AHL* genes, most research has been focused on *AHL* overexpression phenotypes, which are generally similar for different *AHLs*. For example, overexpression of *AHL29/SOB3, AHL27/ESCAROLA/ORE7* and *AHL22* each suppress hypocotyl elongation (Street et al., 2008; Xiao et al., 2009), and overexpression of *AHL15, 19, 20, 22, 27,* or *29* each significantly delays flowering time and promotes plant longevity (Street et al., 2008; Yun et al., 2012; Karami et al., 2020; Tayengwa et al., 2020). The delayed flowering phenotype is caused at least in part by the repression of *FT* expression, suggesting that AHLs can suppress gene expression (Yun et al., 2012; Tayengwa et al., 2020).

Previous studies have shown that *AHL* overexpression affects the chromatin status: Lim et al. (2007) showed that *AHL27* overexpression results in a reduction of chromatin condensation, and Karami et al. (2021) showed that the number of nuclear foci is reduced when *AHL15* is overexpressed and that overexpression of *AHL15* interferes with the proper segregation of sister chromatids specifically during the somatic embryogenesis process, resulting in polyploid embryos. Various studies have shown that acetylation of HISTON 3 (H3Ac) is reduced at specific loci in plants that constitutively overexpress *AHL* genes, whereas its methylation at lysine 9 (H3K9me2) is increased at AHL-bound loci in such plants, suggesting that AHLs promote deposition of repressive epigenetic marks (Ng et al., 2009; Yun et al., 2012; Xu et al., 2013; Xiong et al., 2020). AHLs have been shown to interact with a range of chromatin-modifying proteins, among which several histone deacetylases (HDA) and subunits of the SWR1 complex that exchanges H2A for H2A.Z (Yun et al., 2012; Xu et al., 2013; Lee and Seo, 2017; Xu et al., 2024). A recent study has shown that AHL22 also associates with the transcriptional repressors FRS7 and FRS12 at the matrix attachment regions (MARs) that anchor DNA to the nuclear matrix, and that it recruits the histone deacetylase HDA15 to the DNA (Xu et al., 2024). In addition, RNA-seq datasets show that overexpression of *AHL* proteins causes differential expression of many genes, of which the majority is downregulated (Favero et al., 2020; Karami et al., 2022; Xu et al., 2024). Overall, it is clear that *AHL* overexpression results in differential gene expression, affects chromatin structure, and has a profound effect on plant development. However, the specific mechanisms recruiting AHLs to their target DNA, the direct effect of AHLs on histone modifications,

and the effects of AHLs on chromatin architecture on a global scale remain unclear.

The clade A AHL protein AHL15 has been shown to delay and even reverse developmental phase transitions when overexpressed, thereby extending plant longevity (Karami et al., 2020; Karami et al., 2021; Rahimi et al., 2022a; Rahimi et al., 2022b). Despite the variety of processes in which AHL15 has been shown to play a role, no direct targets of this protein have been identified as of yet. Here, we identified the DNA binding sites of AHL15 in native- and overexpression conditions and investigated the effect of AHL15 on gene expression, chromatin accessibility, and its colocalization with several chromatin modifications. We show that a large set of loci is only bound by AHL15 upon overexpression, and that this coincides predominantly with downregulation of genes. In addition, we show that AHL15 does not affect chromatin accessibility and that it preferentially binds at the boundaries of most epigenetic marks. Finally, we show that AHL15 binding sites largely overlap with those bound by GH1-GMGA2, an AT-hook protein shown to regulate chromatin architecture and gene loop formation (Zhao et al., 2021), implying that AHL15 could play a similar role.

Results

AHL15 binds near the TSS and TES of genes

To identify how AHL15 regulates juvenile plant development, we performed ChIP-seq experiments using a 3xFLAG-tagged AHL15 protein. Because wild-type and *AHL15* overexpressing plants show significant phenotypic differences, we expressed the 3xFLAG-AHL15 fusion protein both in native *(pAHL15:3xFLAG-AHL15* in *ahl15)* and overexpression (*p35S:3xFLAG-AHL15* in Col-0) conditions and pulled down AHL15-bound DNA from both lines (Figure 1A). In wild-type Arabidopsis, *AHL15* is expressed only in juvenile plants and its expression decreases significantly past the seedling stage (Rahimi et al., 2022a). We therefore performed ChIP on 10 day-old seedlings in which the *AHL15* promoter is still strongly active to identify the native DNA binding sites of AHL15. In contrast, *p35S:3xFLAG-AHL15* plants showed a severe delay in flowering time, and overexpression targets were identified in 31 day-old *p35S:3xFLAG-AHL15* plants, which had not yet started to flower at this stage in order to map overexpression-specific targets of AHL15 (Supplementary figure 1).

Our ChIP-seq data show that AHL15 binds DNA abundantly in both native and overexpression conditions (Figure 1A). Under native conditions, we

identified 2425 significant peaks that are shared between both replicates, and an additional 3481 significant peaks in the second replicate, which had a higher sequencing depth (Supplementary data 1). In the overexpression conditions, we identified over 14,000 significant peaks per replicate, of which 10,056 were shared between all three replicates, indicating that AHL15 binds DNA more

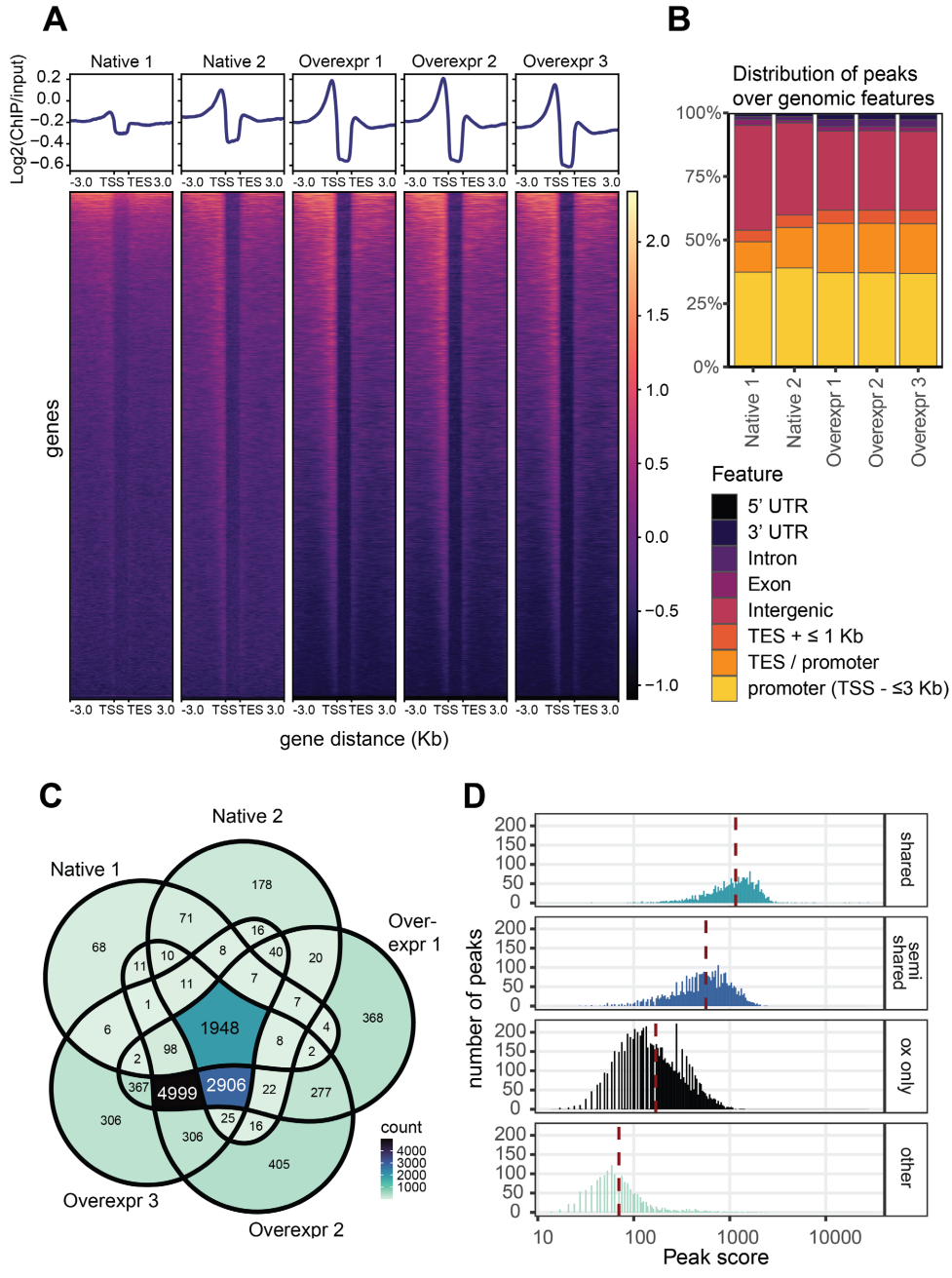

broadly when overexpressed than in wild-type conditions, and that some DNA binding sites are unique to the overexpression condition (Supplementary data 1). Next, we mapped the AHL15 peaks over all genes in the Arabidopsis genome, which showed that AHL15 predominantly binds within 1 kb upstream of the transcription start site (TSS) of genes, and to a lesser extent near the transcription end site (TES) and is depleted over gene bodies (Figure 1A, B). The peak of AHL15 occupancy in these regions was more pronounced in *AHL15* overexpression samples compared to the native condition, showing that AHL15 has a preference for the proximal promoter of genes regardless of whether these are genuine native targets or not. Annotation of the significant AHL15 ChIP-seq peaks over genomic features confirmed that the majority of AHL15 binding sites are located in promoters (up to 3 kb upstream of the TSS) or in intergenic regions (more than 3 kb upstream of the TSS or more than 1 kb downstream of the TES; Figure 1B). In addition, a substantial percentage of AHL15 peaks was located in within 1 kb downstream of the TES or in regions where the promoter and TES of two genes overlapped (TES/promoter; Figure 1B). In overexpression conditions, the share of AHL15 peaks mapping to intergenic regions reduced in favour of promoter- and TES regions, illustrating the increased enrichment of AHL15 near the TSS and TES regions that can be seen in Figure 1A.

To understand what loci are native targets of AHL15 and what loci are unique to the overexpression condition, we compared the significant ChIP

Figure 1 (left page): ChIP-seq of 3xFLAG-AHL15 in native and overexpression conditions. **A:** Heatmap and profile plots of AHL15 ChIP-seq peaks scaled over genes showing that AHL15 is enriched near the TSS and TES, and depleted over gene bodies. Shoots of ten day-old *pAHL15:3x-FLAG-AHL15* were used for ChIP in the native condition, and 31 day-old *p35S:3xFLAG-AHL15* shoots were used for the overexpression condition. Profile plots show the log2 of ChIP reads over input reads. **B:** Annotation of 3xFLAG-AHL15 ChIP-seq peaks in **A** over genomic features of the Araport11 annotation of the Arabidopsis genome. Intergenic: regions that are located more than 3 kb downstream of the TSS or more than 1 kb upstream of the TES and are depleted of genes. TES: region up to 1 kb upstream of the TES. Promoter: region up to 3 kb downstream of the TSS. TES / promoter: regions where promoters overlap with the TES region of neighbouring genes. Intergenic regions are regions not covered by any of the other features. **C:** Venn diagram showing the overlap in peak annotations between the five ChIP-seq samples in **A**. 1948 peaks were identified in all five datasets (*shared*), 2906 peaks were shared between the three overexpression conditions and the second native ChIP (*semi-shared*), and 4999 peaks were identified in all three overexpression (OX) conditions (*OX only*). **D:** Histogram of the peak score of significant ChIP-seq peaks in *p35S:3x-FLAG-AHL15* sample 2 (OX 2). Peaks identified in all five conditions have the highest peak score, followed by semi-shared peaks. OX-only peaks have a lower peak score than shared or semi-shared peaks, and peaks shared in less than 3 conditions have the lowest overall peak score. Reads were aligned with Bowtie2 and peak calling was performed with MACS2.

peaks and identified a set of 1948 loci that are shared between all five ChIP-seq datasets ("shared"; Figure 1C). This set includes the promoters of genes such as *CYTOKININ OXIDASE3 (CKX3), WUSCHEL-RELATED HOMEOBOX 4 (WOX4),* and *TWIN SISTER OF FT (TSF)* (Supplementary data 1). In addition, 2906 peaks were shared between the second replicate of the native ChIP and the three overexpression ChIPs ("semi-shared"), which included promoters of *SQUAMOSA PROMOTER BINDING-LIKE 9 (SPL9)* and *BRANCHED 1 (BRC1)*. We identified 4999 peaks that were common among all three overexpression datasets ("overexpression-only"), that among many others annotated to the promoters of *FLOWERING LOCUST (FT), SWEET10,* and *FLOWERING LOCUS C (FLC)* (Supplementary data 1). When comparing the distribution of peak scores in each category, it was clear that peaks that are shared by all datasets had a higher average peak score than those that are found only in overexpression datasets, indicating that AHL15 binds its native targets more strongly than its ectopic targets (Figure 1D). Thus, these data show that AHL15 can associate with DNA outside of its genuine native binding sites when overexpressed, but that the affinity for these regions is lower than for its native targets.

AHL15 non-specifically binds AT-rich DNA sequences

Because AHLs are known to bind AT-rich DNA and AHL15 binds a large number of promoter regions in both the native and overexpression conditions, we asked whether AHL15 recognizes or binds a specific DNA motif. To this end, we used the motif enrichment analysis tool HOMER (Heinz et al., 2010) to identify enriched motifs in the different datasets: shared, semi-shared, and overexpression-only AHL15 peaks as well as the total of significant peaks of the second overexpression replicate (Figure 2A, Supplementary figures 2-4, Supplementary data 2). Although several AT-rich motifs were found to be significantly enriched in the different datasets, closer inspection showed that the frequency at which these motifs occurred within AHL15 peaks was in most cases less than 1%, making it unlikely to represent a true binding site (Figure 2A, Supplementary figures 2-4). We argued that a true DNA binding motif would be present in a large portion of the AHL15 peaks (targets) and would be rare in other regions of the genome (background). In other words, the motif should have a high target : background ratio and be present in a high percentage of targets. We plotted the target : background ratio (Figure 2B) and the Log2 of the percentage of targets (Figure 2C) values for all significantly enriched *de novo* motifs identified by HOMER for the shared AHL15 peaks. These plots show that most motifs had a high target : background ratio, but

A Enriched motifs of shared peaks

Rank	Motif	P-value	log P-pvalue	% of Targets	% of Background
1		1e-23	-5.488e+01	0.96%	0.01%
2		1e-19	-4.594e+01	0.96%	0.01%
3		1e-15	-3.519e+01	0.67%	0.01%
4		1e-12	-2.937e+01	0.89%	0.04%
5		1e-12	-2.876e+01	0.52%	0.01%
6		1e-12	-2.876e+01	0.52%	0.00%
7		1e-12	-2.876e+01	0.52%	0.01%
8		1e-12	-2.876e+01	0.52%	0.01%

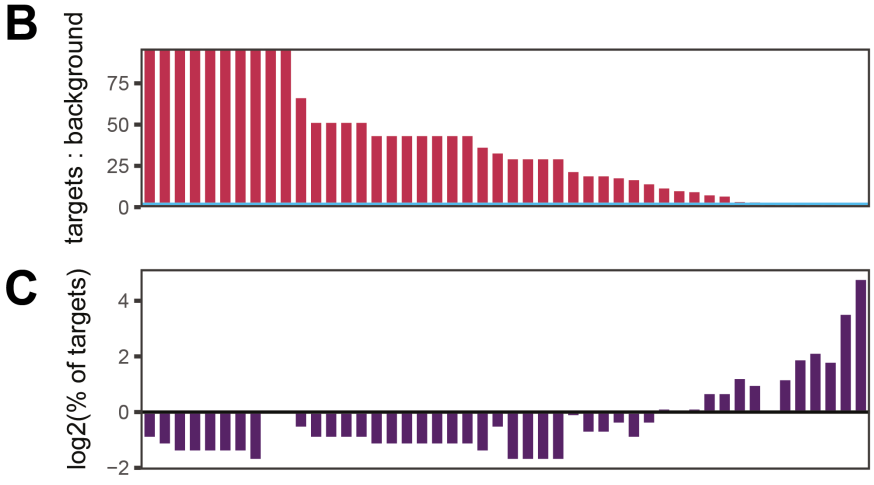

Figure 2: AHL15 binds to AT-rich DNA but does not have a specific DNA binding motif. **A:** Table of the top 8 enriched motifs identified by HOMER2 within the set of shared peaks. **B:** The number of times each motif (48 in total) is identified by HOMER2 in shared AHL15 peaks divided by its number over the entire genome (expressed as %: 100% means the motif is almost only present in AHL15 peaks). **C:** The frequency with which each motif identified by HOMER2 occurs in shared AHL15 peaks, expressed as the Log2 value of the % of shared AHL15 targets containing the specific motif (occurrence of more than 1% gives a positive value, 1% gives a value of 0, and less than 1% results in a negative value). Motifs in figures **B** and **C** are arranged by descending target : background value.

that their occurrence in AHL15 peaks in all such cases was less than 1%. On the other hand, motifs that are present in more than 1% of AHL15 peaks had a low target : background ratio, meaning that these motifs are also common in non-AHL15 bound regions. Similar results were found for each of the AHL15 peak datasets (semi-shared, overexpression-only, and all AHL15 ox rep2 peaks), and no motifs were shared between the four different datasets (Supplementary figures 2-4). Previous research has shown that AHL proteins preferentially bind to AT-rich DNA, and *in vitro* motif discovery experiments suggested several AT-rich sequences as binding sites for AHL proteins (Fujimoto et al., 2004; Franco-Zorrilla et al., 2014). Together, this indicates that AHL15 does not recognize a specific DNA motif but identifies its AT-rich target DNA based on other traits.

Gene expression is predominantly repressed by AHL15

The large number of binding sites we identified in the native and overexpression conditions, as well as the strong phenotypic changes caused by *AHL15* overexpression suggest that AHL15 may regulate the expression of many genes.

To determine which genes are affected by *AHL15* overexpression and may underly the developmental phenotypes associated with *AHL15* overexpression, we used the *p35S:AHL15-GR* line. In this line, a fusion protein of AHL15 and a glucocorticoid receptor (AHL15-GR) is overexpressed, and translocates from the cytosol to the nucleus upon treatment with the steroid hormone dexamethasone (DEX) (Karami et al., 2020). We drenched ten day-old wild type (Col-0) or *p35S:AHL15-GR* seedlings with 20 µM DEX or a mock solution for 15 minutes and harvested seedlings eight hours later for mRNA sequencing. Principal component analysis (PCA) of the RNA-seq data showed that the DEX-

Figure 3 (right page): Genes upregulated by AHL15 show enhanced AHL15 binding at the TSS. **A:** Volcano plot showing differentially expressed genes in 10 day-old *p35S:AHL15-GR* seedlings after 8 hours treatment with DEX compared to the three control conditions (*p35S:AHL15-GR* seedlings treated with mock solution and Col-0 seedlings treated with either DEX or mock solution). Blue dots indicate genes that are significantly more than 2-fold downregulated, red dots indicate genes that are significantly more than 2 fold upregulated, light grey dots show genes that are significantly differentially expressed with a fold change of less than 2, and dark grey dots represent genes whose expression was not significantly altered. **B-D:** Venn diagrams showing overlap of differentially expressed genes with shared ChIP-seq peaks (**B**), semi-shared peaks (**C**), or overexpression-only peaks (**D**). **E:** Table showing a selection of genes shared between ChIP-seq and RNA-seq datasets identified in **B-D**. **F:** Profile plots of AHL15 ChIP-seq peaks over AHL15-bound differentially expressed genes vs all genes. AHL15 enrichment is stronger near the TSS of AHL15-bound differentially expressed genes and especially upregulated genes compared to the average of all genes. Near the TES, AHL15 enrichment is highest for downregulated AHL15-bound genes.

treated *p35S:AHL15-GR* samples grouped at one end, whereas the mock- or DEX-treated Col-0 or the mock-treated *p35S:AHL15-GR* samples grouped at the other end of the PCA plot, showing that DEX treatment had a minimal effect on gene expression in wild type plants compared to *p35S:AHL15-GR* plants (Supplementary figure 5).

Induction of AHL15-GR activity by DEX treatment resulted in a large number of differentially expressed genes, with 1658 genes downregulated over 2-fold and 497 genes upregulated over 2-fold, showing that similar to other *AHL* genes, *AHL15* overexpression causes a net downregulation of gene expression

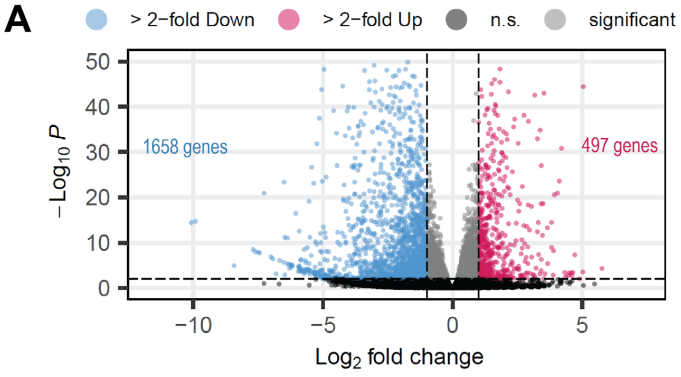

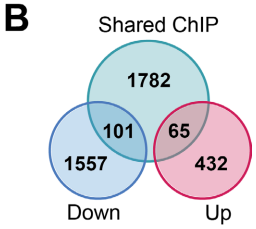

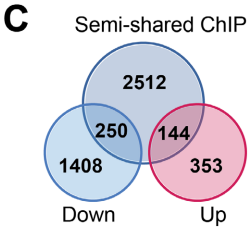

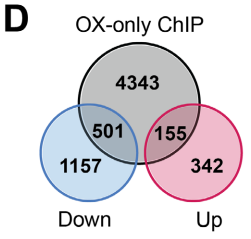

E

	shared		semi-shared		OX only	
	gene	log2FC	gene	log2FC	gene	log2FC
up	TCP16	4.2	JAZ4	2.9	AHP1	2.9
	AHL2	2.8	ANAC042	1.7	HB20	1.7
	GA2OX3	1.3	CLV3	1.3	SMZ	1.3
down	SWEET1	-2.28	BRC1	-1.5	CRC	-2.9
	GA2OX8	-3.1	UFO	-2.20	WOX4	-3.0
	TSF	-3.4	SAUR16	-3.0	BRC2	-4.6
	CKX3	-3.5	FUS3	-3.8	FT	-6.2

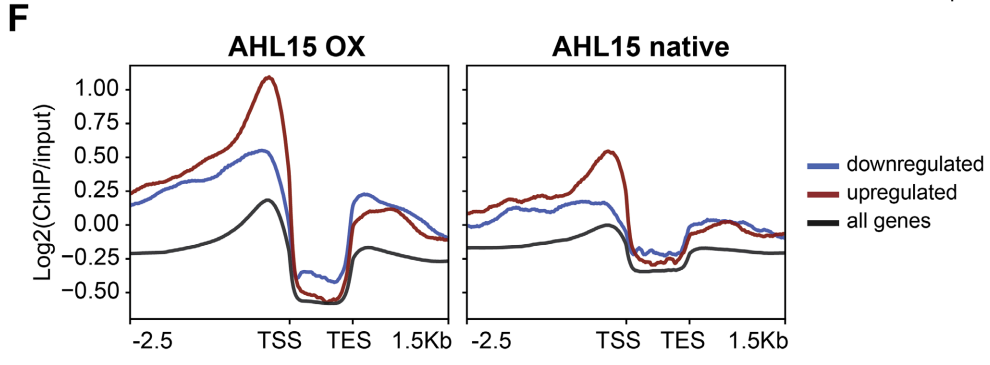

(Figure 3A, Supplementary data 3). Of these, 101 downregulated and 65 upregulated genes were also native targets of AHL15, and 501 downregulated and 155 upregulated genes were overexpression-only targets of AHL15 (Figure 3B-D, Supplementary data 4). A selection of differentially expressed genes that are targeted by AHL15 in native and overexpression conditions is shown in Figure 3E, and includes the flowering-promoting genes *TSF* and *FT* as native and overexpression-only targets, respectively, as well as the meristem maintenance genes *WOX4* and *CLAVATA3* (Fletcher et al., 1999; Ji et al., 2010).

Knowing which genes are differentially expressed upon DEX treatment, we investigated the enrichment of AHL15 ChIP-seq peaks over the differentially expressed genes. To do this, we plotted the average enrichment score of native and overexpression AHL15 ChIP-seq datasets over AHL15-bound upregulated, AHL15-bound downregulated, or all genes. This revealed that AHL15 enrichment was stronger around the TSS and TES of both up- and downregulated genes that were also bound by AHL15 compared to all genes (Figure 3F). Although the majority of differentially expressed genes was downregulated by DEX treatment, and downregulated genes represent a larger fraction of AHL15 DNA binding sites, we observed that AHL15 binding was highest around the TSS of upregulated genes, whereas AHL15 enrichment near the TES was highest for downregulated AHL-bound genes. This suggests that strong AHL15 presence near the TSS of genes may lead to their upregulation, whereas strong AHL15 presence near both the TSS and the TES leads to their downregulation.

Chromatin accessibility is not directly affected by AHL15 induction

Previous research has shown that overexpression of *AHL15* or *AHL27* results in visible changes in chromatin structure (Lim et al., 2007; Karami et al., 2021). , and our ChIP-seq data also show that AHL15 binds to AT-rich DNA with limited sequence specificity throughout the genome. This suggests that AHL15 might alter chromatin accessibility globally. We therefore asked whether the large changes in gene expression we observed upon DEX-induction of AHL15-GR could be a result of altered chromatin accessibility. To test this, we performed ATAC-seq on *p35S:AHL15-GR* seedlings harvested at 30 minutes, 1 hour, and 8 hours after DEX or mock treatment. Surprisingly, we did not observe clear changes in chromatin accessibility at any of the time points: PCA showed that differences between replicates of the same condition were similar or larger than the differences between time points (Figure 4A). For example, ATAC-seq peaks at and around the *FT* locus were similar for all time points, despite a strong downregulation of this gene upon DEX induction (Figure

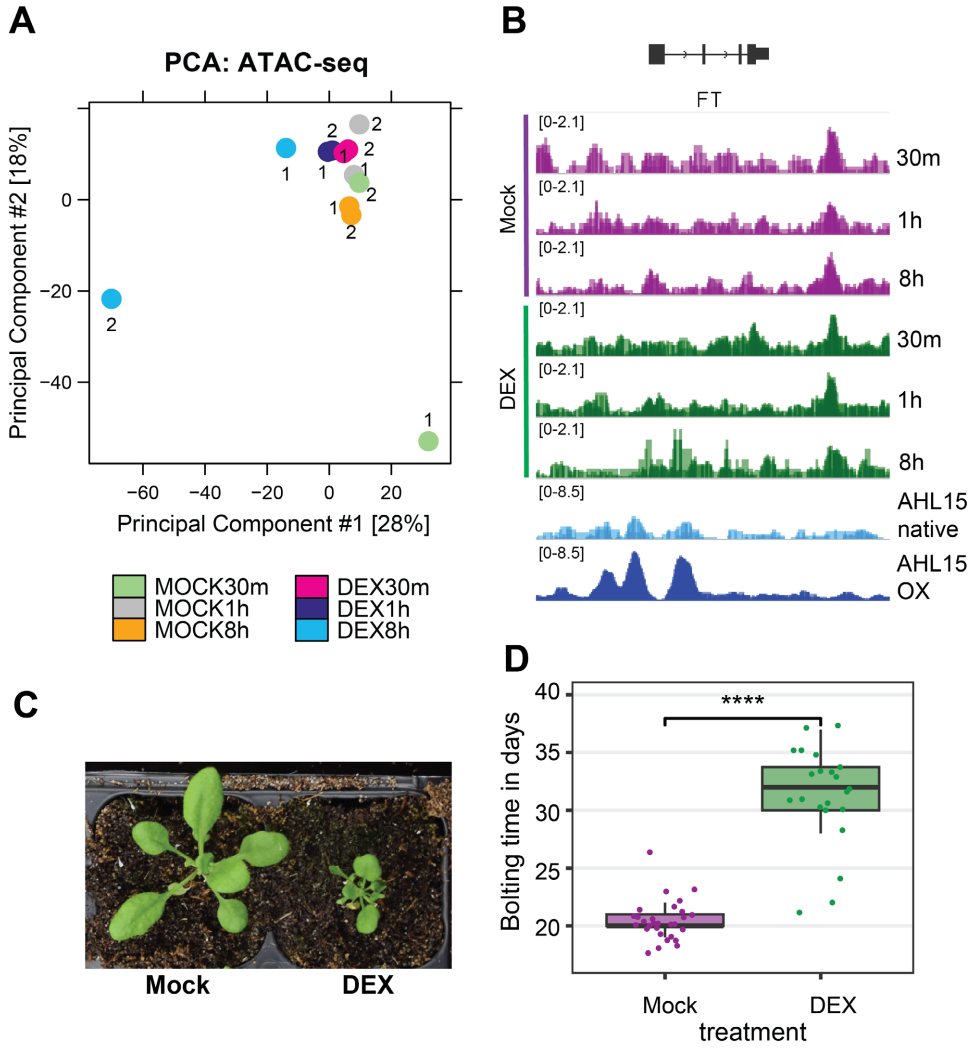

Figure 4: AHL15 delays development but does not affect chromatin accessibility. ATAC-seq of 10 day-old *p35S:AHL15-GR* seedlings that were mock- or DEX treated for 30 minutes, 1 hour or 8 hours. **A:** Principle component analysis of ATAC-seq samples, showing that most samples cluster together and that differences between replicates of the same condition are similar or larger than differences between conditions. **B:** ATAC-seq profiles and AHL15 ChIP-seq profiles at the *FT* locus, a gene that was strongly repressed 8 hours after DEX treatment. Each track shows the overlay of bigwig files from two (ATAC-seq and AHL15 native) or three (AHL15 OX) biological replicates. **C:** Phenotype of mock-treated and DEX-treated *p35S:AHL15-GR* plants at two weeks after DEX treatment (24 day-old plants). Mock-treated plants develop normally and start bolting at this time, whereas DEX-treated plants show an arrested leaf expansion, small stature, and delayed floral transition. **D:** AHL15-GR activation by DEX treatment strongly delays flowering time. Seedlings were transferred to soil two days after DEX treatment and monitored for flowering time (n = 25) and show a significant delay in flowering time (Wilcoxon test, $p = 3.71 \cdot 10^{-9}$). Plants were grown in long day conditions (16 hours light : 8 hours dark).

4B). In addition, we did not detect any differentially accessible regions when comparing DEX- and mock treated samples at the 30m and 1h time points, and identified only 10 regions with differential accessibility for the 8h time point that did not correspond to differentially expressed genes (Supplementary data 5). Although we did not observe clear changes in chromatin accessibility at 8 hours after DEX treatment, the DEX-treated seedlings showed clear phenotypic changes compared to mock-treated seedlings, which resembled the phenotype of *p35S:AHL15* plants (Figure 4C-D; Supplementary figure 1). In addition to a delay in bolting time of about 10 days in DEX-treated plants, new leaves produced at the time of DEX treatment remained very small and did not develop to a full size, resulting in a severe reduction of the plant size. Together with the large number of differentially expressed genes upon DEX treatment, these severe phenotypic changes indicate that AHL15 activation by DEX induces developmental reprogramming. However, our ATAC-seq data indicate that AHL15 does not affect chromatin accessibility directly, and that altered chromatin accessibility cannot explain the differential gene expression patterns observed at the 8h time point and the subsequent developmental reprogramming.

AHL15 binds in regions with reduced epigenetic signatures

Because AHL15 does not have a measurable effect on chromatin accessibility as determined by ATAC-seq, we investigated whether AHL15 binding coincides with epigenetic markers. For this we used publicly available ChIP-seq data of several epigenetic markers in 10 day-old wild-type seedlings (Bourguet et al., 2021). We compared the distribution of these epigenetic markers as well as our ATAC accessibility data with that of AHL15 binding in the native and overexpression conditions by plotting the enrichment of these marks over all Arabidopsis genes (Figure 5). This revealed that AHL15 binding is enriched in regions where chromatin accessibility (based on ATAC seq) is relatively low, and that AHL15 presence is depleted in the highly accessible regions near the TSS and in the gene body (Figure 5A). Similarly, AHL15 showed opposite patterns of enrichment compared to the deposition of H1 (Figure 5B), H2A variants (Figure 5C), and H3K9me1, H3K9me2, and H3K27me1 (Figure 5D). This opposing pattern of enrichment is clearly illustrated when inspecting the sequencing data at individual loci, showing that AHL15 peaks occur at regions where most or all other marks are depleted (Figure 5E). For example, the *TCP16* gene is upregulated in DEX-treated *p35S:AHL15-GR* seedlings, and AHL15 shows clear peaks flanking this gene in both native- and overexpression conditions (Figure

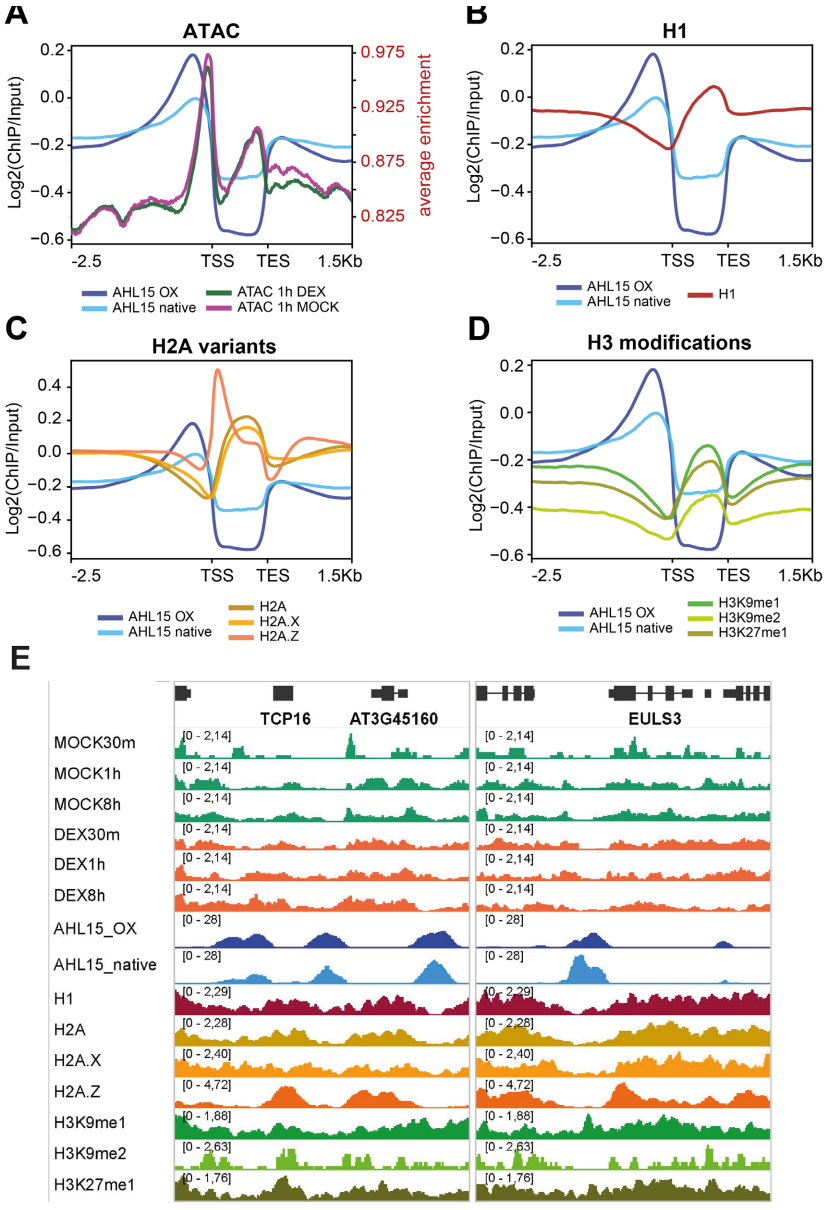

Figure 5: AHL15 binds in regions with reduced accessibility that are depleted of epigenetic marks. **A-D:** ChIP-seq profiles of *pAHL15:3xFLAG-AHL15* (AHL15 native) and *p35S:3xFLAG-AHL15* (AHL15 OX) scaled over all Arabidopsis genes and compared to the ATAC-seq profile of *p35S:AHL15-GR* plants treated with DEX or mock solution for 1 hour (**A**), or to the deposition of Histone 1 (H1) (**B**), Histone 2 variants H2A, H2A.X and H2A.Z (**C**), or the Histone 3 methylation marks H3K9me1, H3K9me2, and H3K27me1 (**D**). **E:** Alignment of the AHL15 native (AHL15_native) and overexpression (AHL15_OX) ChIP-seq profiles at the *TCP16* and *EULS3* loci with the averaged ATAC-seq profiles of ten day-old *p35S:AHL15-GR* seedlings that were mock- or DEX treated for 30 minutes, 1 hour or 8 hours and the epigenetic marks shown in **B-D**.

5E). At regions where AHL15 peaks are visible, a clear reduction in ATAC peaks and H2A.Z, and to a lesser extent H2A, H2A.X, H1, H3K9me1, H3K9me2, and H3K27me1 deposition can be seen. A similar pattern could be observed for all epigenetic marks except H3K9me1, and to a lesser extent H3K27me3, around the AHL15 peak near the *EULS3* locus, whose expression was unaffected by DEX treatment (Figure 5E). These patterns are also visible when plotting the enrichment of epigenetic marks around AHL15 ChIP-seq peaks. This analysis shows that chromatin accessibility (based on ATAC-seq) is reduced around the centre of AHL15 ChIP-seq peaks, and this reduction is most clear around strong AHL15 ChIP-seq peaks that were identified in both the native and overexpression condition and less pronounced around overexpression-only AHL15 peaks (Figure 6). H2A, H2A.X, H2A.Z, and H1 deposition is also depleted most strongly around shared AHL15 peaks (Figure 7), and H3K27me1 and H3K9me2 are both depleted around AHL15 peaks, but less strongly at shared AHL15 peaks than at overexpression-only peaks. Finally, H3K9me1 shows a slight enrichment at shared and semi-shared AHL15 peaks, illustrated by the peak seen at the *EULS3* locus (Figures 5E, 7E). Taken together, these analyses clearly show that AHL15 binds at regions that are depleted of most epigenetic marks, which could be explained in different ways. First, it is possible that AHL15 is repelled by the presence of specific marks such as H2A.Z, and therefore binds only in regions where these marks are absent. Alternatively, it is possible that AHL15 has a preference for regions with reduced chromatin accessibility, which would explain the opposing patterns of AHL15 binding and ATAC-seq peaks. A third possibility is that AHL15 binding results in the removal of the deposition of epigenetic marks, but the depletion of most histone modifications around overexpression-specific AHL15 peaks does not support this idea.

AHL15 binds genes at both ends and may be involved in gene looping

AHL15 binds predominantly near the TSS of genes and is also enriched near the TES (Figure 1[1]A, B, Figure 5E), indicating that its presence at both ends of genes may be inherent to its mechanism of transcriptional regulation. Like AHL proteins, members of the globular H1 domain containing high-mobility group A (GH1-HMGA) protein family have AT-hook DNA-binding domains that bind the minor groove of AT-rich DNA and can affect local chromatin structure (García-Heras et al., 2009; Ozturk et al., 2014; Charbonnel et al., 2018). It was shown that GH1-HMGA proteins bind at both the 5′ and 3′ end of the *FLC* locus and thereby disrupt the formation of a gene loop associated with active transcription, resulting in a reduced transcription of *FLC* and an accelerated flowering time

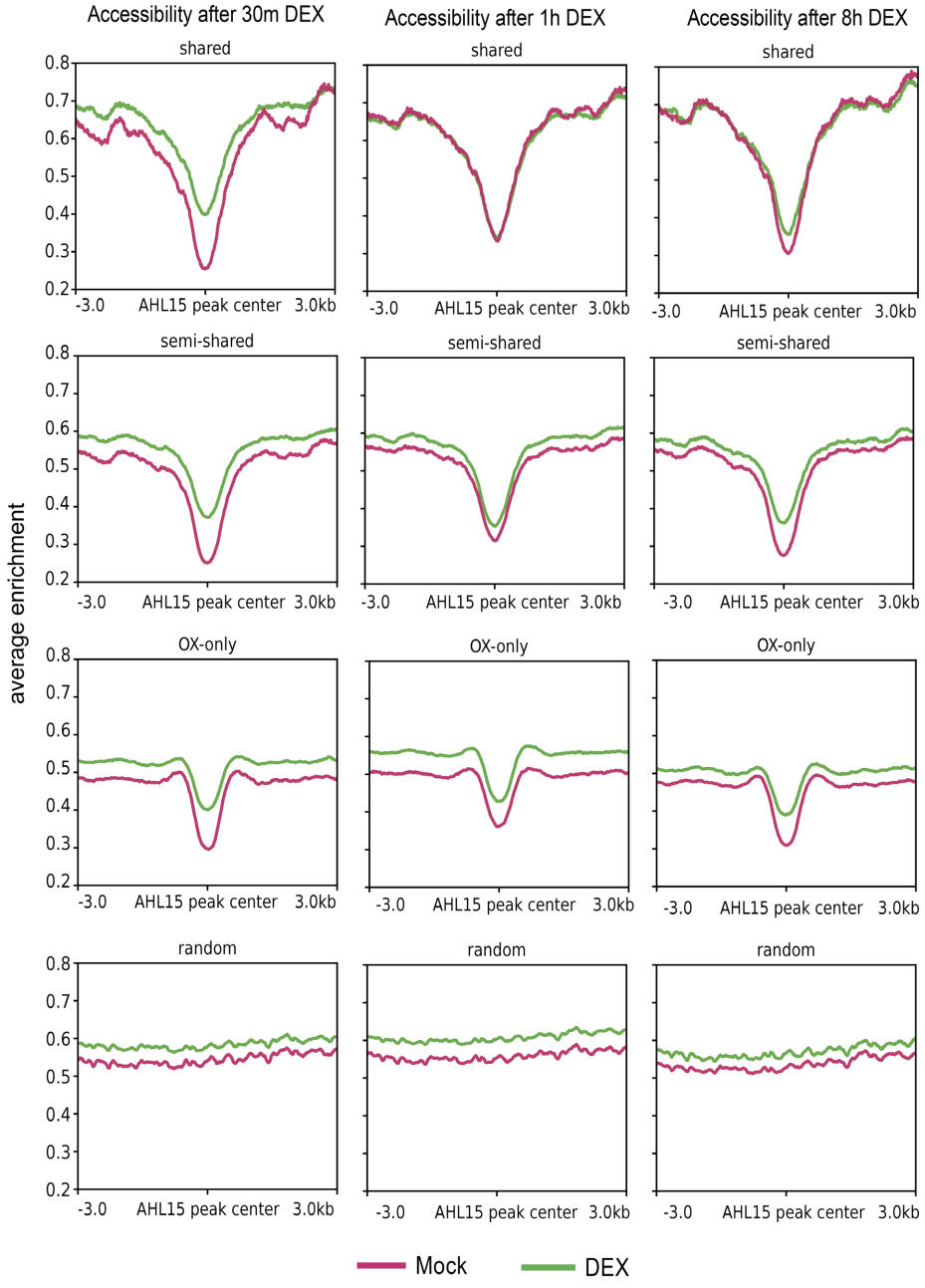

Figure 6: Chromatin accessibility is reduced around AHL15 binding sites. ATAC-seq reads from *p35S:AHL15-GR* plants treated with DEX or mock for 30 minutes, 1 hour or 8 hours were plotted over three classes of AHL15 ChIP-seq peaks presented in Figure 1C: shared (identified in native and overexpression conditions, n = 1948), semi-shared (identified in one native sample and in all overexpression samples, n = 2906), and OX-only (identified in all three overexpression samples, n = 4999). Random genomic coordinates with similar size distribution as the ChIP-seq peaks were used as a negative control (random, n = 15221 regions).

(Zhao et al., 2021). As AHL and GH1-HMGA proteins share the same type of DNA-binding domain, and because AHL15 peaks also flank genes at both ends, we compared our AHL15 ChIP-seq data to previously published ChIP-seq data of GH1-HMGA2/HON5. GH1-HMGA2/HON5 is enriched near the TSS and

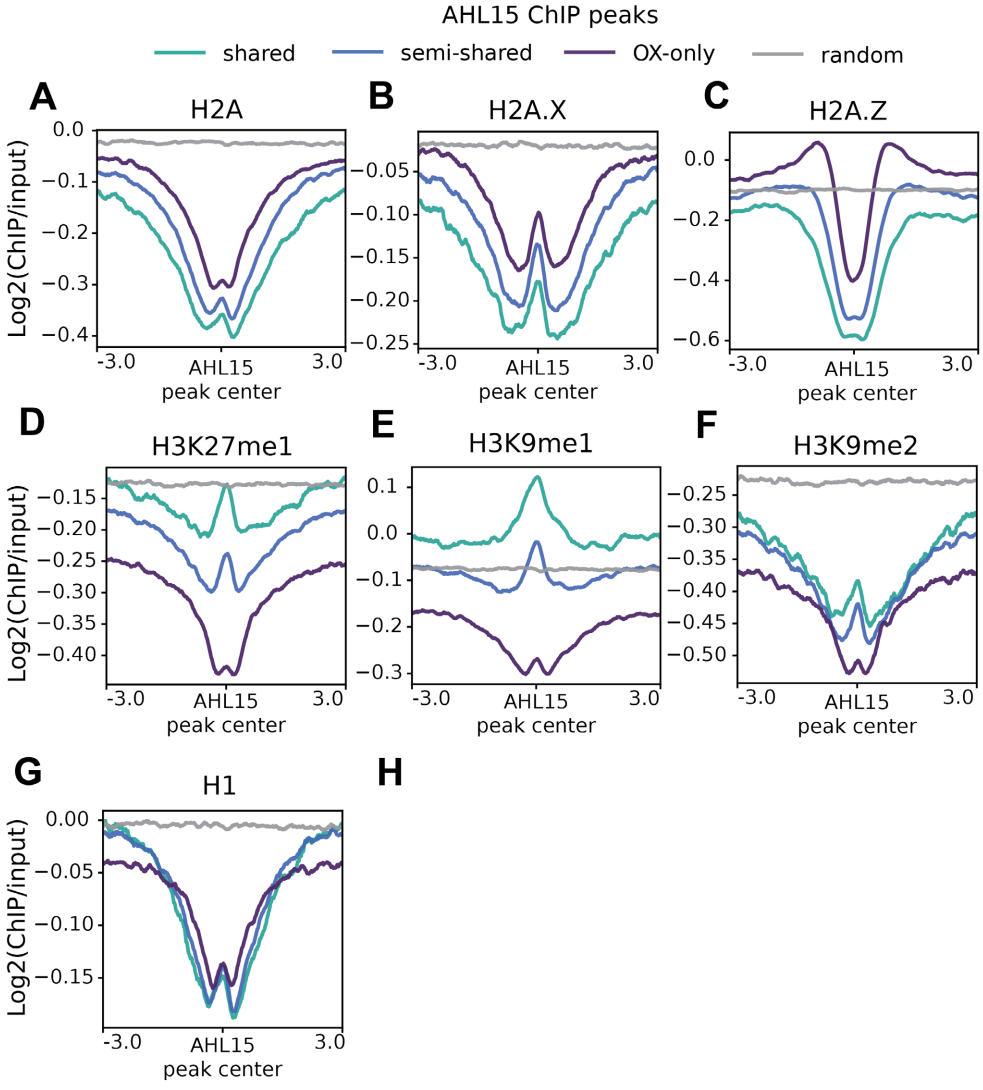

Figure 7: Epigenetic marks are depleted around AHL15 binding sites. **A-G:** ChIP-seq profiles for the epigenetic marks H2A (**A**), H2A.X (**B**), H2A.Z **(C),** H3K27me1 (**D**), H3K9me1 (**E**), H3K9me2 (**F**), and H1 (**G**) were plotted over three classes of AHL15 ChIP-seq peaks presented in Figure 1C: shared (identified in native and overexpression conditions, n = 1948), semi-shared (identified in one native sample and in all overexpression samples, n = 2906), and OX-only (identified in all three overexpression samples, n = 4999). Random genomic coordinates with similar size distribution as the ChIP-seq peaks were used as a negative control (random, n = 15221 regions).

TES of genes in a similar pattern as AHL15, indicating that both proteins may bind at the same position (Figure 8A). To test this, we plotted the enrichment of GH1-HMGA2/HON5 ChIP-seq reads over AHL15 peaks, and found that GH1-HMGA2/HON5 reads are strongly enriched at these positions (Figure 8B). GH1-HMGA2/HON5 binding is strongest at canonical AHL15 binding sites, as it was most enriched at shared AHL15 peaks and weaker at overexpression-only peaks. Comparison of AHL15 and GH1-HMGA2/HON5 enrichment at specific loci further confirmed that they bind at the same position: the GH1-HMGA2/HON55 peak near the TSS of *FLC* was also present in the AHL15 overexpression datasets, as well as a weaker peak near the *FLC* TES (Figure 8C). Similarly, both GH1-HMGA2/HON5 and AHL15 bind at both ends of the self-looping gene *RCD1,* which was also upregulated upon AHL15-GR activation by DEX (Figure 8C). Finally, we compared the AHL15 ChIP-seq data with 1766 previously identified self-looping genes, and found that AHL15 binding at self-looping genes is significantly enhanced in overexpression conditions compared to native conditions (Figure 8D). In addition, at least 91 AHL15-bound self-looping genes were also upregulated, and 77 AHL15-bound self-looping genes were downregulated upon DEX treatment (Figure 8E, Supplementary data 6). Taken together, these comparisons show that like GH1-HMGA proteins, AHL15 is likely to be involved in regulating gene loop formation and may affect the expression of its target genes in this way.

Discussion

Overexpression of various *AHL* genes, and in particular *AHL15,* has been shown to induce developmental reprogramming, causing a delay or even reversal of ageing-related developmental transitions such as vegetative phase change, the floral transition and leaf senescence (Lim et al., 2007; Street et al., 2008; Karami et al., 2020; Karami et al., 2021; Rahimi et al., 2022a; this thesis chapter 4). However, the mechanism causing these developmental changes remained unclear so far. Here, we mapped the genome-wide DNA binding sites of AHL15, and show that AHL15 binds throughout the genome at regions near the TSS and TES and is depleted in gene bodies. Our data show that when overexpressed, AHL15 is present at many ectopic binding sites, and also binds more strongly at its native targets. Despite the clear positional preference of AHL15 for regions upstream of the TSS and downstream of the TES, we did not identify a convincingly conserved binding motif, as the most frequently occurring motifs enriched in AHL15-bound regions also show high occurrence in the genomic background. This suggests that while they show a

clear preference for AT-rich DNA, AHL15 and likely other AHL proteins as well do not recognize specific DNA sequences, but are rather recruited to their AT-rich target sites in a different way.

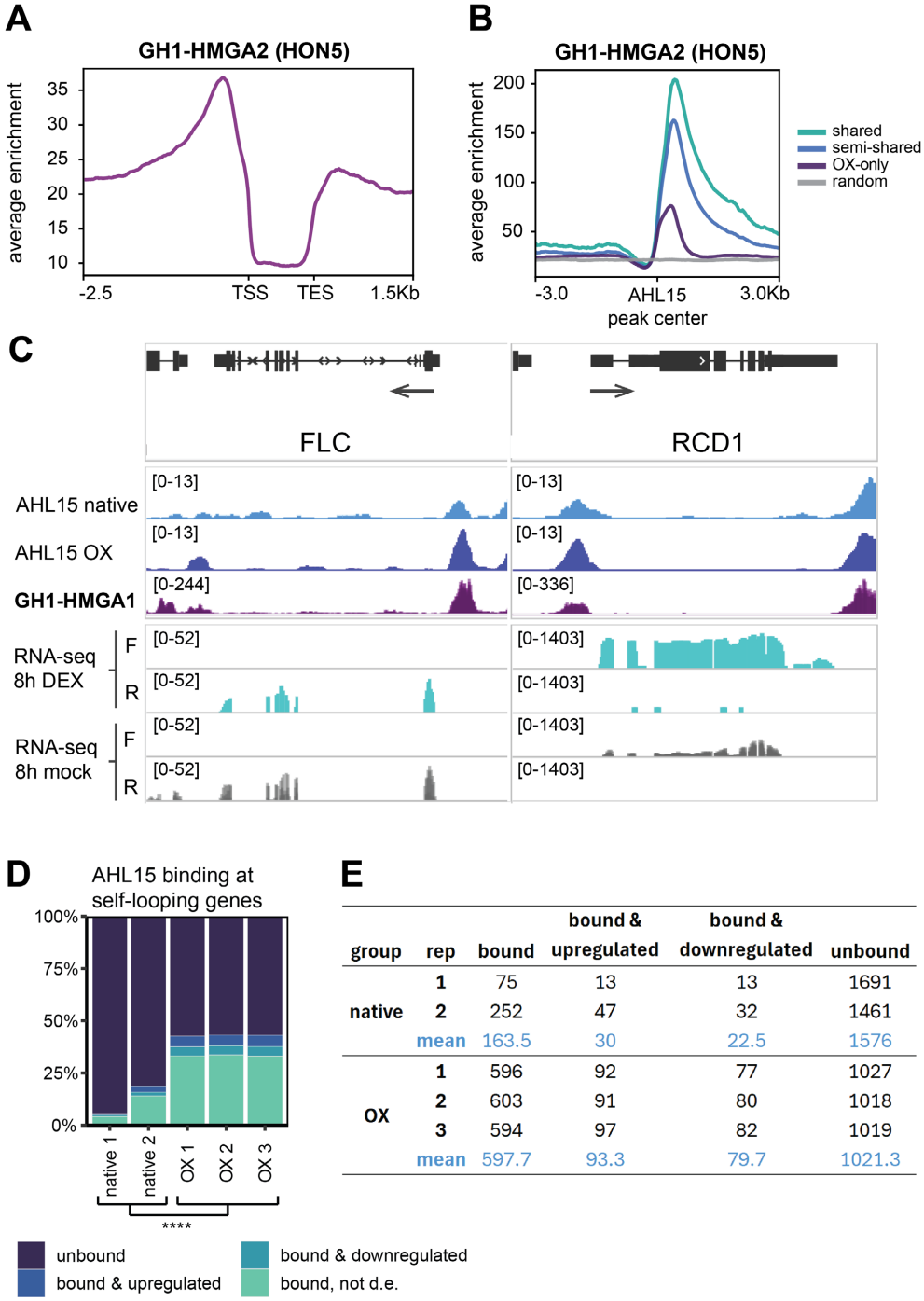

E

group	rep	bound	bound & upregulated	bound & downregulated	unbound
native	1	75	13	13	1691
	2	252	47	32	1461
	mean	163.5	30	22.5	1576
OX	1	596	92	77	1027
	2	603	91	80	1018
	3	594	97	82	1019
	mean	597.7	93.3	79.7	1021.3

Our experiments with the DEX-inducible *p35S:AHL15-GR* line show that *AHL15* overexpression causes strong transcriptional and phenotypic changes, with a majority of differentially expressed genes being downregulated. About one third of these differentially expressed genes was also bound by AHL15, indicating that AHL15 directly regulates the expression of a large number of genes. However, ATAC-seq in the same conditions showed that the changes in transcriptome induced by AHL15-GR activation do not coincide with changes in chromatin accessibility, suggesting that AHL15 regulates transcriptional activation or repression in an accessibility-independent manner. We also compared the positions of AHL15 peaks with ATAC-generated accessibility data, and saw that AHL15 binds regions with relatively low accessibility, just before the highly accessible region around the TSS. As AHL15-GR activation by DEX treatment did not cause changes in the ATAC-seq profile within 8 hours, it is likely that AHL15 binding does not reduce chromatin accessibility itself, but is rather recruited to regions with reduced accessibility. However, it remains unclear what attracts AHL15 or other AHL proteins to a specific locus.

We also investigated whether AHL15 peaks overlap with heterochromatin-associated epigenetic marks such as H1, H3K9me1, and H3K9me2, and observed a clear pattern in which AHL15 flanked most of these marks. AHL proteins were initially discovered as components of the nuclear matrix, and AHL1 was shown to localize at the boundary between heterochromatic regions and H3K4me-marked regions (Fujimoto et al., 2004). Our data show that AHL15 similarly flanks other epigenetic signatures, as we saw no overlap of AHL15 with any mark except a weak overlap with H3K9me1 deposition. It is likely

Figure 8 (left page): AHL15 binds at the same positions as the GH1-HMGA family protein HON5 and may be involved in gene looping. **A:** Profile plot of GH1-HMGA2/HON5 ChIP-seq reads scaled over Arabidopsis genes showing a similar enrichment pattern as AHL15. **B:** GH1-HMGA2/HON5 ChIP-seq reads are were plotted over three classes of AHL15 ChIP-seq peaks presented in Figure 1C shared (identified in native and overexpression conditions, n = 1948), semi-shared (identified in one native sample and in all overexpression samples, n = 2906), and OX-only (identified in all three overexpression samples, n = 4999). **C:** AHL15 and GH1-HMGA2/HON5 ChIP-seq peaks around the *FLC* and *RCD1* loci. ChIP-seq and RNA-seq tracks show an average of biological replicates of the same condition. RNA-seq tracks indicate mapped reads per strand; the *FLC* gene is located on the reverse strand (R) and *RCD1* is located on the forward (F) strand. **D:** AHL15 binding to self-looping genes increases when overexpressed. Percentages of self-looping genes that are not bound by AHL15, bound by AHL15 and are upregulated upon DEX treatment, bound by AHL15 and downregulated upon DEX treatment, and bound by AHL15 but not differentially expressed (d.e.) are shown for each AHL15 ChIP-seq sample. The number of self-looping genes that are bound by AHL15 increases significantly in overexpression samples compared to native samples (X^2 test, $p < 0.0001$). **E:** Table showing the number of self-looping genes in each category shown in **D.**

that AHL15 preferentially binds to regions devoid of epigenetic marks, but we cannot exclude the possibility that AHL15 induces removal of some histone variants or epigenetic modifications, for example that of H2A.Z or H1, which were both more depleted around shared (native and OX) AHL15 peaks than around OX-only peaks. Previous studies have shown that overexpression of different clade A *AHLs* results in increased H3K9me2 and decreased H3Ac deposition at the *FT* and *FLC* loci (Ng et al., 2009; Yun et al., 2012; Xu et al., 2013), but these findings are likely to represent indirect effects of enhanced *AHL* expression rather than direct effects of AHL binding to the loci that were investigated. Genome-wide profiling of epigenetic marks in DEX-induced and non-induced AHL15-GR plants should give conclusive evidence of the effect of AHL15, and by proxy other AHLs, on the deposition of epigenetic marks.

Interestingly, AHL15 peaks overlap with those of GH1-HMGA2/HON5, a protein that was previously shown to interfere with gene loop formation between the 5′ and 3′ ends of the *FLC* locus, thereby hindering *FLC* transcription (Zhao et al., 2021). The similarity in DNA-binding domains between AHL15 and GH1-HMGA2/HON5 explains their overlap in DNA binding sites, and suggests that AHL15 may play a similar role as GH1-HMGA2/HON5 in regulating loop formation. HMGA-family proteins contain four AT-hook domains, whereas clade A AHLs have a single AT-hook domain (Klosterman and Hadwiger, 2002; Zhao et al., 2014). AHLs are known to form complexes with themselves and with other AHLs (Zhao et al., 2013), resulting in a complex that contains three AT-hooks, and this property could be necessary to bind AT-rich DNA with sufficient strength to affect its 3D confirmation. This could explain the strong effect of dominant-negative AHL alleles on the phenotype: the absence of an AT-hook domain in ΔAT-hook variants likely reduces the affinity for DNA of the entire AHL complex they are part of, thereby reducing the potential of entire complexes to bind DNA and modify its architecture. On the other hand, AHL complexes that incorporate the ΔG variant can still bind DNA, but have a reduced ability to recruit interacting proteins that could be required to alter the chromatin architecture. In both cases, the reduced ability of AHL complexes to affect DNA structure likely interferes with the proper regulation of gene expression, explaining the strong phenotypes observed in dominant-negative mutants (Zhao et al., 2013; Karami et al., 2020; Karami et al., 2021). In addition, AHL complexes and HMGAs might compete for the same regions in the DNA and have an effect on gene loop formation via association with different interaction partners. Although the expression of *FLC* was not affected in DEX-treated seedlings, several other self-looping genes were differentially

expressed upon AHL15-GR activation. It would therefore be interesting to study whether these previously reported self-loops are altered upon AHL15-GR activation, whether AHL15 facilitates or disrupts these loops, and whether this results in altered transcription at these loci.

Previous research has shown that TFs that activate gene expression preferentially bind to regions near the TSS, whereas repressors are more likely to bind both near the TSS and near the TES (Franco-Zorrilla et al., 2014). In line with this, we observed that AHL15 enrichment was enhanced around the TSS of AHL15-bound upregulated genes, whereas enrichment near the TES was highest for AHL15-bound downregulated genes. This suggests that strong association of AHL15 with the TSS of genes relative to the TES enhances their expression and that a more equal distribution of AHL15 binding near the TSS and TES represses their expression. However, the effect of AHL15 binding at these regions on gene loop formation remains unclear.

Finally, our ATAC-seq data shows that AHL15 does not directly affect chromatin accessibility. This result is surprising, as earlier reports have shown that overexpression of *AHL15* or *AHL27* causes visible changes in the intensity of heterochromatin foci in the nucleus, suggesting a reduced chromatin compaction (Lim et al., 2007; Karami et al., 2021). It is possible that AHL15 induces chromatin opening on a slower time scale than measured here, but our finding that AHL15 may act similar to GH1-HMGA2/HON5 in the 3D organization of DNA could offer an alternative explanation for this phenomenon. GH1-HMGA2/HON5 was shown to disrupt chromatin looping on a local scale, but the authors did not investigate the effect of this protein on the global 3D structure of the DNA (Zhao et al., 2021). As chromatin architectural modifiers, it is likely that both GH1-HMGA and AHL proteins can affect chromatin looping on short-range as well as long-range scales. Here, we have shown that AHL15 binds in regions depleted in histone modifications and other epigenetic signatures, and similarly, AHL1 was shown to be present at the boundaries between H3K4me-marked euchromatin and DAPI-stained heterochromatin foci (Fujimoto et al., 2004). It is therefore possible that excessive AHL presence alters or disrupts these boundaries, causing changes in heterochromatin compartmentalization that result in the disappearance of heterochromatin foci that is observed in *AHL* overexpression lines (Lim et al., 2007; Karami et al., 2021).

Materials & methods

Plant material and growth conditions

The Arabidopsis *p35S:AHL15-GR* line and *ahl15* (SALK_040729) loss-of-function mutant have been described previously (Karami et al., 2020). *p35S:3xFLAG-AHL15* or *pAHL15:3xFLAG-AHL15* constructs were cloned into the binary vector pMDC32 (Karimi et al., 2007) and transformed to Arabidopsis by floral dip (Clough and Bent, 1998). Overexpression constructs were expressed in the Col-0 background and *pAHL15:3xFLAG-AHL15* was expressed in the *ahl15* loss-of-function mutant background, and only plants homozygous for the T-DNA insertion were used for experiments. Seeds were sterilized in 2% sodium hypochlorite for 2 minutes and washed with sterile milliQ water (mQ) before plating on ½ MS medium and then stratified for three days at 4 °C. For seedling experiments, plates were placed vertically in a growth chamber and grown for 10 days in long-day conditions (16h light/8h dark) at 21 °C. For overexpression ChIP, *p35S:3xFLAG-AHL15* seedlings were grown on ½ MS with 15 mg/L kanamycin for 10 days and then transferred to soil and grown in a growth chamber at 21 °C with long-day conditions for an additional 21 days prior to harvesting whole shoots for ChIP.

ChIP-seq

The ChIP protocol used was adapted from the protocols by Kaufmann et al. (2010) and Chouaref et al. (2018). For each ChIP, 1 g of shoot tissue from 31 day-old *35S:3xFLAG-AHL15* or 10 day-old *pAHL15:3xFLAG-AHL15* plants was harvested and fixated for 10 minutes on ice and under vacuum in 1% formaldehyde in ice-cold MC buffer (10 mM sodium phosphate buffer pH 7, 50 mM NaCl, 0.1 M sucrose). The fixation reaction was stopped by saturation with glycine, and samples were washed in ice-cold MC buffer, dried with tissue paper, and stored at -80 °C. For nuclei isolation, frozen fixated tissue was ground to a very fine powder in liquid nitrogen using a mortar and pestle, and was then resuspended in 15 mL M1 buffer (10 mM sodium phosphate buffer pH 7, 0.1 M NaCl, 1 M 2-methyl 2,4-pentanediol, 10 mM β-mercaptoethanol) and gently shaken at 4 °C for 30 minutes. Suspensions were subsequently filtered through respectively a 100 µM and a 70 µM nylon mesh, both of which were washed with an additional 5 mL M1 buffer to extract remaining nuclei. The filtered suspension was then centrifuged for 20 minutes at 1000x*g* at 4°C, and pellets were resuspended in 20 mL M2 buffer (10 mM sodium phosphate buffer

pH 7, 0.1 M NaCl, 1 M 2-methyl 2,4-pentanediol, 10 mM β-mercaptoethanol, 10 mM $MgCl_2$, 0.5% Triton X-100). After 30 minutes of gentle shaking at 4 °C, the suspension was centrifuged for 10 minutes at 1000x*g* at 4 °C, the supernatant was discarded and the pellet was resuspended again in 5 mL M2 buffer. After 10 minutes of gentle shaking followed by 10 minutes centrifugation at 1000x*g* at 4 °C, the pellet was resuspended in 1 mL sonication buffer (10 mM sodium phosphate buffer pH 7, 0.1 M NaCl, 0.5% Sarkosyl, 10 mM EDTA) and aliquoted to 300 µL in 1.5 mL protein lobind tubes (Eppendorf, Germany). Samples were then sonicated in a Bioruptor sonicator (Diagenode, Seraing, Belgium) on HIGH for 5 rounds of 10 cycles of 30 seconds ON / 30 seconds OFF to a fragment size of ~300 bp. After sonication, tubes of the same replicate were pooled and spun for 10 minutes at 12000x*g at* 4 °C, and the supernatant was transferred to a new tube and stored at -20 °C.

For the immunoprecipitation, 50 µg chromatin was used per IP (ca 250 µL sonicated material), and 3.5 volumes IP buffer (50 mM HEPES pH 7.5, 150 mM NaCl, 5 mM $MgCl_2$, 10 µM $ZnSO_4$, 1% Triton X-100, 0.05% SDS) and 25 µL protein G dynabeads (ThermoFischer, Lithuania) conjugated to mouse monoclonal Anti-FLAG M2 antibodies (F1804; Sigma-Aldrich, Darmstadt, Germany) were added and rotated at 4 °C overnight. After this, beads were washed once in 1 mL of each of the following buffers: IP buffer, high salt buffer (500 mM NaCl, 0.1% SDS, 1% Triton X-100, 2 mM EDTA, 20 mM Tris-HCl pH 8), LiCl buffer (10 mM Tris-HCl pH 8, 1 mM EDTA, 1% NP-40, 1% sodium deoxycholate, 0.25 M LiCl), and twice in TE buffer (10 mM Tris-HCl pH 8, 1 mM EDTA), and then resuspended in 50 µL TE buffer. Samples were decrosslinked overnight at 65 °C after adding 450 µL of decrosslinking buffer (50 mM Tris-HCl pH 8, 10 mM EDTA pH 8, 250 mM NaCl, 1 % (w/v) SDS). DNA was cleaned by phenol: chloroform extraction, ethanol precipitated, and resuspended in milliQ and treated with RNAse A (ThermoScientific, Vilnius, Lithuania) for 30 minutes at 37 °C, and then stored at -20 °C until sequencing. ChIP samples were sequenced with the Illumina Novaseq 6000 at Macrogen (Amsterdam, the Netherlands) with 20 million 150 bp paired-end reads.

RNA-seq

Ten day-old seedlings (Col-0 and *p35S:AHL15-GR*) were flooded at zeitgeber time 1 with 35 mL 20 µM DEX in milliQ or with a mock solution with an equivalent volume of DMSO for 15 minutes, after which the solution was siphoned off. The plates were returned to the growth chambers and five seedlings per replicate (n=3) of each condition (*p35S:AHL15-GR* + DEX, *p35S:AHL15-GR* + mock, Col-

0 + DEX, Col-0 + mock) were harvested (shoot only) after eight hours and snap-frozen in liquid nitrogen. The frozen plant material was pulverized with a metal bead in a Tissuelyser (Qiagen, Hilden, Germany) and RNA was isolated using Trizol© (ThermoFischer, Vilnius, Lithuania) with an additional ethanol wash step. For sequencing, 3 µg RNA was aliquoted and treated with DNAse-I (ThermoFischer, Vilnius, Lithuania) for 30 minutes at 37 °C. Library preparation and sequencing with the Illumina Novaseq 6000 (150 bp paired-end, 10 million reads) was done at Baseclear (Leiden, the Netherlands).

ATAC-seq

Seedlings were treated with DEX or mock solution as for RNA-seq. For each replicate, approximately 50 DEX- or mock-treated seedlings were harvested (shoot only) at 30 minutes, 1 hour, or 8 hours after treatment, dried, and snap-frozen in liquid nitrogen and stored at -80 °C. Nuclei isolation was done by chopping frozen seedlings on ice in 2 mL nuclei isolation buffer (INGR) and subsequent filtering through a 40 µM mesh according to the protocol by Wang et al. (2021). Nuclei were diluted 5-fold in nuclei isolation buffer and stained with propidium iodide. 55,000 nuclei were sorted per sample using the S3e Cell Sorter (Bio-Rad, Hercules, USA) with FSC = 365 and SSC = 299. Nuclei were subsequently pelleted and Tagmentation and library amplification was done using the Zymo-seq ATAC library kit (D5458, Zymo Research, Irvine, USA). Sequencing was done with the Illumina Novaseq 6000 (150 bp paired-end, 20 million reads) at Baseclear (Leiden, the Netherlands).

Bioinformatic analysis

ChIP-seq, RNA-seq, and ATAC-seq analyses were done with Nextflow using the NF core ChIP-seq, ATAC-seq, or RNA-seq pipelines (Ewels et al., 2020), and reads were mapped to the TAIR10 Arabidopsis genome annotation. The threshold for peak identification by MACS2 in the NF core pipeline was lowered to $p < 0.05$ for ATAC-seq samples due to a low library complexity in these samples. For ChIP, reads were annotated in R using the ChIPSeeker package (Yu et al., 2015; Wang et al., 2022), and differential expression analysis for RNA-seq and differential accessibility analysis for ATAC-seq was done using the DESeq2 package (Love et al., 2014). Differentially expressed genes were calculated by comparing the DEX-treated *p35S:AHL15-GR* condition with the three control conditions (*p35S:AHL15-GR* + mock, Col-0 + mock and Col-0 + DEX), as the difference between control conditions was sufficiently small to exclude a strong effect

of DEX on gene expression in Col-0 (Supplementary Figure 5). For ATAC-seq, mock- and DEX-treated samples at the same time point were compared.

Heatmaps of ChIP-seq reads were generated using deepTools (Ramírez et al., 2016). To annotate ChIP-seq peaks over genomic features, we used BEDTools (Quinlan and Hall, 2010) to categorize the TAIR10 genome into non-overlapping regions of the following categories: promoters (0-3 kb upstream of TSS), TES (0-1 kb downstream of TES), TES and promoter (regions where promoters and TES of adjacent genes overlapped), exon, intron, 5′ UTR, 3′ UTR, and intergenic (regions that are not covered by any of the other categories). Overlap between ChIP-seq and RNA-seq datasets was calculated in R, and ChIP-seq peaks shared between all AHL15 datasets, shared between 4/5 AHL15 datasets, or unique to the overexpression datasets were identified using R and exported as BED files for further comparisons. Additionally, the ChIP peak coordinates of one *AHL15* overexpression ChIP-seq dataset were shuffled over the Arabidopsis genome to generate a set of random peak coordinates as a control. Motif enrichment analyses and de novo motif finding were done using HOMER2 (Heinz et al., 2010).

For the analysis of ChIP-seq data of epigenetic marks, raw data of epigenetic markers in wild type plants generated by Bourguet et al. (2021) was downloaded from GEO and re-analyzed with the NF core ChIP-seq pipeline. For generating profile plots of the various epigenetic marks over Arabidopsis genes or the AHL15 peaks, bigwig files of individual replicates were first normalized to input using a log2 normalization method and subsequently averaged before calculation of the count matrices and profile plotting with deepTools.

Acknowledgements

We thank Jan Vink, Altay Temel, Ward de Winter and Mariel Lavrijsen for technical support and Alex Bos, Marjolein Crooijmans and Dennis Claessen for help with nuclear sorting for ATAC-seq. We thank Salma Balazadeh for sharing her ChIP-seq protocol and Maike Stam for her advice on the ATAC-seq experiment.

Literature

Bourguet P., Picard C.L., Yelagandula R., Pélissier T., Lorković Z.J., Feng S., Pouch-Pélissier M.N., Schmücker A., Jacobsen S.E., Berger F., et al (2021). The histone variant H2A.W and linker histone H1 co-regulate heterochromatin accessibility and DNA methylation. Nat Commun **12**: 1–12.

Charbonnel C., Rymarenko O., Ines O. Da, Benyahya F., White C.I., Butter F., Amiard S. (2018). The linker histone GH1-HMGA1 is involved in telomere stability and DNA damage repair. Plant Physiol **177**: 311–327.

Chouaref J., de Boer E., Fransz P., Stam M. (2018). Protocol for chromatin immunoprecipitation of meiotic-stage-specific tomato anthers. Curr Protoc Plant Biol **3**: e20074.

Clough S.J., Bent A.F. (1998). Floral dip: a simplified method for *Agrobacterium*-mediated transformation of *Arabidopsis thaliana*. Plant J **16**: 735–743.

Ewels P.A., Peltzer A., Fillinger S., Patel H., Alneberg J., Wilm A., Garcia M.U., Di Tommaso P., Nahnsen S. (2020). The nf-core framework for community-curated bioinformatics pipelines. Nat Biotech **38**: 276–278.

Favero D.S., Kawamura A., Shibata M., Takebayashi A., Jung J.H., Suzuki T., Jaeger K.E., Ishida T., Iwase A., Wigge P.A., et al (2020). AT-Hook transcription factors restrict petiole growth by antagonizing PIFs. Curr Biol **30**: 1454–1466.

Fletcher J.C., Brand U., Running M.P., Simon R., Meyerowitz E.M. (1999). Signaling of cell fate decisions by CLAVATA3 in Arabidopsis shoot meristems. Science (1979) **283**: 1911–1914.

Franco-Zorrilla J.M., López-Vidriero I., Carrasco J.L., Godoy M., Vera P., Solano R. (2014). DNA-binding specificities of plant transcription factors and their potential to define target genes. PNAS **111**: 2367–2372.

Fujimoto S., Matsunaga S., Yonemura M., Uchiyama S., Azuma T., Fukui K. (2004). Identification of a novel plant MAR DNA binding protein localized on chromosomal surfaces. Plant Mol Biol **56**: 225–239.

García-Heras F., Padmanabhan S., Murillo F.J., Elías-Arnanz M. (2009). Functional equivalence of HMGA- and histone H1-like domains in a bacterial transcriptional factor. PNAS **106**: 13546–13551.

Heinz S., Benner C., Spann N., Bertolino E., Lin Y.C., Laslo P., Cheng J.X., Murre C., Singh H., Glass C.K. (2010). Simple combinations of lineage-determining transcription factors prime cis-regulatory elements required for macrophage and B cell identities. Mol Cell **38**: 576–89.

Ji J., Strable J., Shimizu R., Koenig D., Sinha N., Scanlon M.J. (2010). WOX4 promotes procambial development. Plant Physiol **152**: 1346–1356.

Karami O., Henkel C., Offringa R. (2022). The effect of short-term activation of AHL15 on long-term plant developmental change and transcriptome profile. bioRxiv 2022.09.05.506087.

Karami O., Rahimi A., Khan M., Bemer M., Hazarika R.R., Mak P., Compier M., van Noort V., Offringa R. (2020). A suppressor of axillary meristem maturation promotes longevity in flowering plants. Nat Plants **6**: 368–376.

Karami O., Rahimi A., Mak P., Horstman A., Boutilier K., Compier M., van der Zaal B., Offringa R. (2021). An Arabidopsis AT-hook motif nuclear protein mediates somatic embryogenesis and coinciding genome duplication. Nat Commun **12**: 2508.

Karimi M., Depicker A., Hilson P. (2007). Recombinational Cloning with Plant Gateway Vectors. Plant Physiol **145**: 1144–1154.

Kaufmann K., Muiño J.M., Østerås M., Farinelli L., Krajewski P., Angenent G.C. (2010). Chromatin immunoprecipitation (ChIP) of plant transcription factors followed by sequencing (ChIP-SEQ) or hybridization to whole genome arrays (ChIP-CHIP). Nat Protoc **5**: 457–472.

Kim H.B., Oh C.J., Park Y.C., Lee Y., Choe S., An C.S., Choi S.B. (2011). Comprehensive analysis of *AHL* homologous genes encoding AT-hook motif nuclear localized protein in rice. BMB Rep **44**: 680–685.

Klosterman S.J., Hadwiger L.A. (2002). Plant HMG proteins bearing the AT-hook motif. Plant Science **162**: 855–866.

Kumar A., Singh S., Mishra A. (2023). Genome-wide identification and analyses of the AHL gene family in rice (*Oryza sativa*). 3 Biotech. doi: 10.1007/s13205-023-03666-0

Lee K., Seo P.J. (2017). Coordination of matrix attachment and ATP-dependent chromatin remodeling regulate auxin biosynthesis and Arabidopsis hypocotyl elongation. PLoS One **12**: 1–19.

Lim P.O., Kim Y., Breeze E., Koo J.C., Woo H.R., Ryu J.S., Park D.H., Beynon J., Tabrett A., Buchanan-Wollaston V., et al (2007). Overexpression of a chromatin architecture-controlling AT-hook protein extends leaf longevity and increases the post-harvest storage life of plants. Plant J **52**: 1140–1153.

Lin L., Nakano H., Nakamura S., Uchiyama S., Fujimoto S., Matsunaga S., Kobayashi Y., Ohkubo T., Fukui K. (2007). Crystal structure of *Pyrococcus horikoshii* PPC protein at 1.60 Å resolution. Proteins: Structure, Function, and Bioinformatics **67**: 505–507.

Love M.I., Huber W., Anders S. (2014). Moderated estimation of fold change and dispersion for RNA-seq data with DESeq2. Genome Biol **15**: 550.

Machaj G., Grzebelus D. (2021). Characteristics of the *at-hook motif containing nuclear localized (AHL)* genes in carrot provides insight into their role in plant growth and storage root development. Genes (Basel) **12**: 764.

Ng K.H., Yu H., Ito T. (2009). AGAMOUS controls GIANT KILLER, a multifunctional chromatin modifier in reproductive organ patterning and differentiation. PLoS Biol **7**: e1000251.

Ozturk N., Singh I., Mehta A., Braun T., Barreto G. (2014). HMGA proteins as

modulators of chromatin structure during transcriptional activation. Front Cell Dev Biol **2**: 1–9.

Quinlan A.R., Hall I.M. (2010). BEDTools: a flexible suite of utilities for comparing genomic features. Bioinformatics **26**: 841.

Rahimi A., Karami O., Balazadeh S., Offringa R. (2022a). miR156 -independent repression of the ageing pathway by longevity-promoting AHL proteins in Arabidopsis. New Phytol **235**: 2424–2438.

Rahimi A., Karami O., Lestari A.D., de Werk T., Amakorová P., Shi D., Novák O., Greb T., Offringa R. (2022b). Control of cambium initiation and activity in Arabidopsis by the transcriptional regulator AHL15. Curr Biol **32**: 1764–1775.

Ramírez F., Ryan D.P., Grüning B., Bhardwaj V., Kilpert F., Richter A.S., Heyne S., Dündar F., Manke T. (2016). deepTools2: a next generation web server for deep-sequencing data analysis. Nucleic Acids Res **44**: W160–W165.

Street I.H., Shah P.K., Smith A.M., Avery N., Neff M.M. (2008). The AT-hook-containing proteins SOB3/AHL29 and ESC/AHL27 are negative modulators of hypocotyl growth in Arabidopsis. Plant Journal **54**: 1–14.

Tayengwa R., Sharma Koirala P., Pierce C.F., Werner B.E., Neff M.M. (2020). Overexpression of *AtAHL20* causes delayed flowering in Arabidopsis via repression of *FT* expression. BMC Plant Biol **20**: 559.

Wang F.X., Shang G.D., Wu L.Y., Mai Y.X., Gao J., Xu Z.G., Wang J.W. (2021). Protocol for assaying chromatin accessibility using ATAC-seq in plants. STAR Protoc. doi: 10.1016/j.xpro.2020.100289

Wang Q., Li M., Wu T., Zhan L., Li L., Chen M., Xie W., Xie Z., Hu E., Xu S., et al (2022). Exploring Epigenomic Datasets by ChIPseeker. Curr protoc **2**: e585.

Xiao C., Chen F., Yu X., Lin C., Fu Y.F. (2009). Over-expression of an *AT-hook gene, AHL22*, delays flowering and inhibits the elongation of the hypocotyl in *Arabidopsis thaliana*. Plant Mol Biol **71**: 39–50.

Xiong S.X., Zeng Q.Y., Hou J.Q., Hou L.L., Zhu J., Yang M., Yang Z.N., Lou Y. (2020). The temporal regulation of TEK contributes to pollen wall exine patterning. PLoS Genet **16**: e1008807.

Xu L., Zheng S., Witzel K., Van De Slijke E., Baekelandt A., Mylle E., Van Damme D., Cheng J., De Jaeger G., Inzé D., et al (2024). Chromatin attachment to the nuclear matrix represses hypocotyl elongation in *Arabidopsis thaliana*. Nat Commun **15**: 1286.

Xu Y., Wang Y., Stroud H., Gu X., Sun B., Gan E.S., Ng K.H., Jacobsen S.E., He Y., Ito T. (2013). A matrix protein silences transposons and repeats through interaction with retinoblastoma-associated proteins. Curr Biol **23**: 345–350.

Yu G., Wang L.G., He Q.Y. (2015). ChIPseeker: an R/Bioconductor package for ChIP peak annotation, comparison and visualization. Bioinformatics **31**: 2382–2383.

Yun J., Kim Y.-S., Jung J.-H., Seo P.J., Park C.-M. (2012). The AT-hook motif-containing protein AHL22 regulates flowering initiation by modifying

FLOWERING LOCUS T chromatin in Arabidopsis. J Biol Chem **287**: 15307–15316.

Zhao B., Xi Y., Kim J., Sung S. (2021). Chromatin architectural proteins regulate flowering time by precluding gene looping. Sci Adv **7**: 3097–3108.

Zhao J., Favero D.S., Peng H., Neff M.M. (2013). *Arabidopsis thaliana AHL* family modulates hypocotyl growth redundantly by interacting with each other via the PPC/DUF296 domain. PNAS **110**: E4688–E4697.

Zhao J., Favero D.S., Qiu J., Roalson E.H., Neff M.M. (2014). Insights into the evolution and diversification of the *AT-hook Motif Nuclear Localized* gene family in land plants. BMC Plant Biol **14**: 1–19.

Zhou J., Wang X., Lee J.Y., Lee J.Y. (2013). Cell-to-cell movement of two interacting AT-Hook factors in Arabidopsis root vascular tissue patterning. Plant Cell **25**: 187–201.

Supplementary figures

Supplementary figure 1: Phenotype of 31 day-old *p35S:3xFLAG-AHL15* plants right before harvesting for ChIP. White arrowheads mark plants with particularly strong AHL15-induced delay of development. Plants were grown in LD (16h light / 8h dark), and the scale on the bottom of the image is in cm.

Supplementary figure 2 (right page): HOMER de novo motif finding results calculated based on all AHL15 peaks (shared, semi-shared, and overexpression-only). **A:** Table of the top 20 enriched motifs identified by HOMER2 within all AHL15 peaks. **B:** The number of times each motif (75 in total) is identified by HOMER2 in all AHL15 peaks divided by its number over the entire genome (expressed as %: 100% means the motif is almost only present in AHL15 peaks). **C:** The frequency with which each motif identified by HOMER2 occurs in all AHL15 peaks, expressed as the Log2 value of the % of shared AHL15 targets containing the specific motif (occurrence of more than 1% gives a positive value, 1% gives a value of 0, and less than 1% results in a negative value). Motifs in figures **B** and **C** are arranged by descending target : background value.

A

Total target sequences = 12083
Total background sequences = 40333
* - possible false positive

Rank	Motif	P-value	log P-pvalue	% of Targets	% of Background	STD(Bg STD)
1		1e-23	-5.519e+01	0.17%	0.01%	11.2bp (9.9bp)
2		1e-18	-4.155e+01	0.14%	0.01%	9.2bp (6.3bp)
3		1e-18	-4.155e+01	0.14%	0.01%	11.5bp (4.2bp)
4		1e-17	-4.087e+01	0.16%	0.01%	13.7bp (10.2bp)
5		1e-17	-3.948e+01	0.18%	0.02%	11.2bp (7.8bp)
6		1e-16	-3.828e+01	0.13%	0.01%	9.1bp (19.7bp)
7		1e-16	-3.789e+01	0.15%	0.01%	12.5bp (15.6bp)
8		1e-15	-3.573e+01	0.24%	0.03%	14.2bp (13.1bp)
9		1e-15	-3.506e+01	0.12%	0.01%	13.0bp (8.1bp)
10		1e-15	-3.506e+01	0.12%	0.01%	8.1bp (1.6bp)
11		1e-15	-3.496e+01	0.14%	0.01%	11.2bp (10.9bp)
12		1e-14	-3.322e+01	0.41%	0.11%	12.1bp (15.7bp)
13		1e-14	-3.269e+01	0.18%	0.02%	10.5bp (11.0bp)
14		1e-13	-3.192e+01	0.12%	0.01%	12.3bp (17.4bp)
15		1e-13	-3.177e+01	0.16%	0.02%	10.5bp (8.9bp)
16		1e-13	-3.173e+01	0.21%	0.03%	12.8bp (14.7bp)
17		1e-13	-3.170e+01	3.14%	2.08%	12.2bp (13.9bp)
18		1e-12	-2.779e+01	0.13%	0.01%	13.0bp (3.4bp)
19		1e-12	-2.778e+01	0.18%	0.03%	12.6bp (10.0bp)
20 *		1e-11	-2.663e+01	0.22%	0.04%	12.9bp (12.6bp)

B

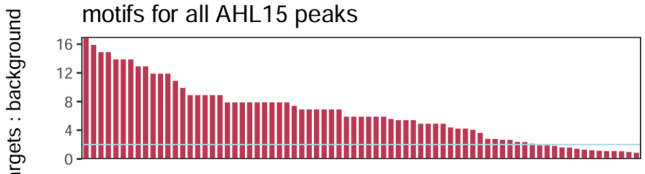

C

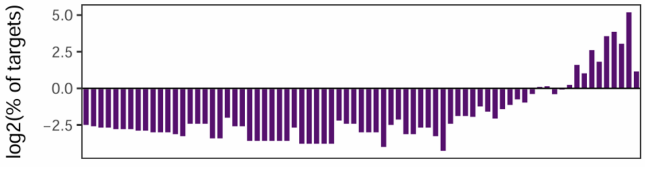

A

Total target sequences = 6522
Total background sequences = 40000
* - possible false positive

Rank	Motif	P-value	log P-pvalue	% of Targets	% of Background	STD(Bg STD)
1		1e-18	-4.268e+01	0.18%	0.00%	15.2bp (0.8bp)
2		1e-18	-4.248e+01	0.26%	0.01%	12.1bp (3.0bp)
3		1e-15	-3.572e+01	0.24%	0.01%	12.4bp (14.4bp)
4		1e-14	-3.451e+01	0.18%	0.01%	14.1bp (10.8bp)
5		1e-14	-3.404e+01	0.15%	0.00%	9.3bp (6.5bp)
6		1e-12	-2.985e+01	0.14%	0.00%	7.6bp (0.0bp)
7		1e-12	-2.871e+01	0.59%	0.14%	10.8bp (13.2bp)
8 *		1e-11	-2.605e+01	0.23%	0.02%	8.6bp (20.3bp)

B

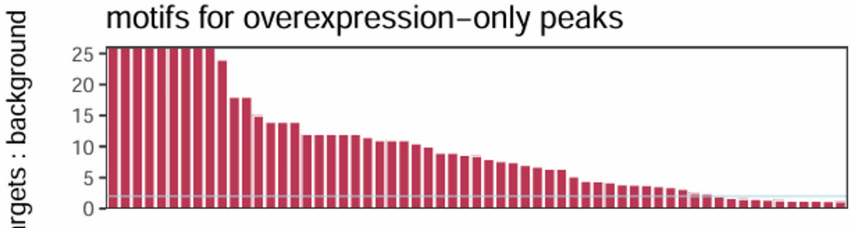

C

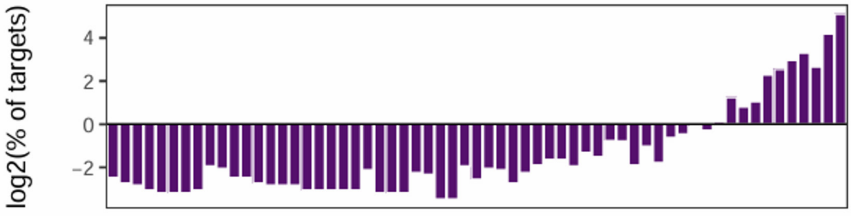

Supplementary figure 3: HOMER de novo motif finding results for overexpression-only peaks. **A:** Table of the top 8 enriched motifs identified by HOMER2 within the set of overexpression-only peaks. **B:** The number of times each motif (61 in total) is identified by HOMER2 in overexpression-only AHL15 peaks divided by its number over the entire genome (expressed as %: 100% means the motif is almost only present in AHL15 peaks). **C:** The frequency with which each motif identified by HOMER2 occurs in overexpression-only AHL15 peaks, expressed as the Log2 value of the % of shared AHL15 targets containing the specific motif (occurrence of more than 1% gives a positive value, 1% gives a value of 0, and less than 1% results in a negative value). Motifs in figures **B** and **C** are arranged by descending target : background value.

A

Total target sequences = 4000
Total background sequences = 51667
* - possible false positive

Rank	Motif	P-value	log P-pvalue	% of Targets	% of Background	STD(Bg STD)
1		1e-19	-4.398e+01	0.38%	0.01%	10.8bp (9.3bp)
2		1e-15	-3.683e+01	0.28%	0.01%	10.2bp (5.9bp)
3		1e-14	-3.269e+01	0.25%	0.01%	9.5bp (10.4bp)
4		1e-14	-3.263e+01	0.35%	0.02%	13.7bp (12.0bp)
5		1e-13	-3.124e+01	8.03%	5.18%	11.4bp (13.0bp)
6		1e-13	-3.017e+01	0.20%	0.00%	8.2bp (0.0bp)
7		1e-13	-3.017e+01	0.20%	0.00%	10.6bp (1.7bp)
8		1e-12	-2.937e+01	0.28%	0.01%	12.7bp (14.0bp)
9		1e-12	-2.872e+01	0.25%	0.01%	9.2bp (10.2bp)
10		1e-12	-2.864e+01	0.23%	0.01%	11.5bp (7.6bp)
11 *		1e-11	-2.592e+01	0.25%	0.01%	10.4bp (5.8bp)

B

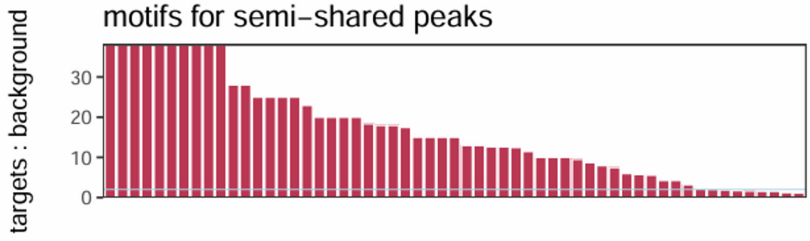

C

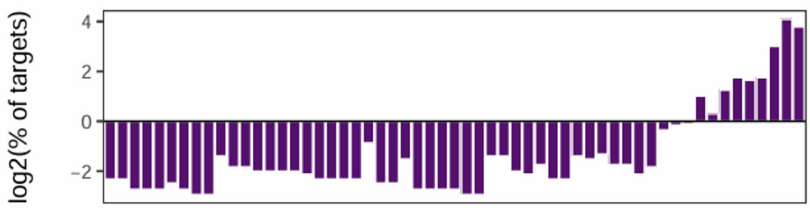

Supplementary figure 4: HOMER de novo motif finding results for semi-shared peaks. **A:** Table of the top 11 enriched motifs identified by HOMER2 within the set of semi-shared peaks. **B:** The number of times each motif (57 in total) is identified by HOMER2 in semi-shared AHL15 peaks divided by its number over the entire genome (expressed as %: 100% means the motif is almost only present in AHL15 peaks). **C:** The frequency with which each motif identified by HOMER2 occurs in semi-shared AHL15 peaks, expressed as the Log2 value of the % of shared AHL15 targets containing the specific motif (occurrence of more than 1% gives a positive value, 1% gives a value of 0, and less than 1% results in a negative value). Motifs in figures **B** and **C** are arranged by descending target : background value.

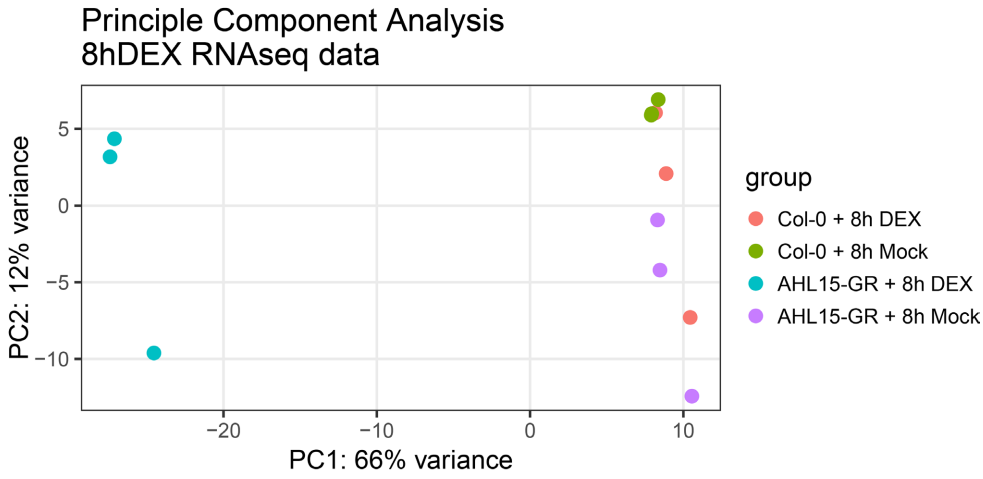

Supplementary figure 5: Principle component analysis of RNA-seq datasets. RNA-seq was performed on RNA isolated from 10 day-old wild-type (Col-0) or *p35S:AHL15-GR* seedlings that were drenched in 20 µM DEX or mock solution for 15 minutes, after which the DEX solution was removed and plants were left to recover. Per replicate (n=3) shoot tissue of five plants was harvested at 8 hours after drenching for RNA isolation and sequencing.